Final Draft
of the original manuscript:

Huber, N.; Heerens, J.:
On the effect of a general residual stress state on indentation and hardness testing
In: Acta Materialia (2008) Elsevier

DOI: 10.1016/j.actamat.2008.08.029

On the effect of a general residual stress state on indentation and hardness testing

N. Huber[1], J. Heerens

GKSS Research Centre Geesthacht, Institute of Materials Research, Materials Mechanics, Max-Planck-Strasse 1, 21502 Geesthacht, Germany

Keywords: hardness test; nanoindentation; residual stresses; yield phenomena; analytical methods

Abstract

Residual stresses superimpose the stress field from an indentation experiment and do therefore influence the measurement of the volume of interest. The residual stress state can be very different in magnitude and biaxiality and error that may be caused in the measured hardness is difficult to estimate. A prediction of the pressure ratio for stressed and unstressed material is carried out by new model that accounts for nonlinearities caused by the von Mises flow rule. The model can also be used for the correction of the effect of a general residual stress state before further analysis of the measured indentation data towards the underlying mechanical properties, such as the stress-strain behaviour. The model does further allow estimating the measurement uncertainty when the stress ratio or the strength of the material is unknown, which is a typical scenario for hardness testing in welded steels and aluminium alloys.

[1] Corresponding Author: norbert.huber@gkss.de, Phone: +49-4152-87-2500, Fax: +49-4152-87-2534

1. Introduction

Residual stresses play an important role in many technological applications. Depending on how residual stresses superimpose external loads, they can influence the mechanical behaviour and therefore, the lifetime of components in a positive or in a negative manner, i.e. compressive residual stresses on the surface are positive since they make it more difficult to initiate in particular fatigue cracks. Disadvantageous effects of residual stresses in metals are afflicted with highly varying stress gradients, e.g. in the vicinity of welded joints, as an adverse effect of the dimensional accuracy of a component due to distortion. Residual stresses can reach the magnitude of the yield limit and can therefore cause plastic deformations. The control and minimization of residual stresses through the production process is therefore an important technological challenge.

It is however often impossible to eliminate residual stresses, particularly when post heat treatment is too expensive or when it would destroy the well-designed microstructure of the component. At the same time, the investigation of the local property variation either after production or during service is very important for the reliability assessment of a component. Since depth and force sensing indentation systems have become a standard technique, a strong development of theoretical models and numerical procedures can be observed in this field.

It has been shown experimentally [1] as well as by finite element simulations [2] for various alloys that internal uniaxial or biaxial stresses influence hardness measurement results. It was found that the hardness decreases with internal tensile stresses and vice versa. However, the effect of internal compressive stresses is not as large as that of internal tensile stresses, i.e. the effect is non-linear. Motivated by pure shear plasticity theory, which decides for different slip planes in case of tensile

and compressive residual stress, Tsui et al. fitted the measured change in hardness versus the applied stress data by a bilinear relationship with a higher sensitivity for tensile stresses.

To estimate the effect of residual stresses and to develop models for its description, it is possible to compare indentation or contact depth [3], indentation force [4], unload behaviour [5], contact area [6], pile-up [7], or hardness [1] with and without residual stress.

Suresh and Giannakopoulos [6] proposed a model, where a differential contact force is added in direction of the applied normal force in order to mimic the effect of an equibiaxial stress state through a hydrostatic stress plus a differential stress. They introduced the von Mises effective yield stress and accounted for its increase through the plastic deformation by common power law hardening. Only the residual stress components are considered while the normal stress component, which represents the contact pressure, was set to zero. Their theoretical model is specific for sharp indenters, such as Vickers or Berkovich tips, and is restricted to equibiaxial residual stress states. It should be pointed out that the resulting smooth curve describing the real contact area as a function of the residual stress agrees with the nonlinear trend from compression to tension, which has been observed earlier by Tsui et al.

Swadener et al. [8] proposed two methods for spherical indentation based on the onset of yielding and the contact pressure. The first approach requires the yield stress of the material to be known independently, as well as a very smooth surface or a very large indenter radius in the experiment. The latter one is based on the empirical observation that the curve representing mean contact pressure versus normalized contact radius are vertically shifted by an amount very close to the applied biaxial stress, as compared to the unstressed material. This means that

Swadener et al. observed a linear relationship between an equibiaxial residual stress and the resulting mean contact pressure.

Carlsson and Larsson [7] recognized that the residual compression stress enhanced the pile-up and was thus misleading in plastic contact area determination, while residual tension stress reduced the plastic contact area. As a result of their investigation, they found that the increase in the contact area can be estimated by the simple relation $A/A_{nom} = c^2 = 1 - \sigma^{(res)}/(3\sigma_y)$. Beside the experimental validation in the second part of their work [9] Carlsson and Larsson mentioned that a direct extension of the equibiaxial results to a general solution would be to determine the apparent yield stress, when an indentation induced compressive and equi-biaxial stress field is superimposed over the surface residual stresses in the material, using the von Mises yield criterion. In contrast to Suresh and Giannakopoulos, the normal stress component has not been set to zero. Instead Carlsson and Larsson suggested to use the apparent yield stress $\sigma(\varepsilon_{res})$ at the corresponding representative strain. However, Carlsson and Larsson did not provide a solution for a general residual stress state as it can also be seen in later articles [10,11], where they used the same equation as it is given above.

Lee, Kwon and co-workers modified the idea of Suresh and Giannakopoulos, by simply interpreting the effect of the residual stress as the normal component in the resulting deviatoric part of the stress tensor [3,12] and found that the contribution of an equibiaxial residual stress $\sigma^{(res)}$ on the indentation force is $P_{res} = -(2/3)\sigma^{(res)} A_C^T$, where P_{res} is the contribution to the indentation force caused by the residual stress and A_C^T is the real contact area in the tensile stress state. In subsequent work [12-14] they extended and validated their deviatoric stress model towards a general residual stress state by introducing the stress ratio κ into the previous equation, so that

$P_{res} = -(1+\kappa)/3 \cdot \sigma^{(res)} A_C^T$. Experiments were in good agreement with this relation, although it cannot predict the known nonlinearities reported by Tsui et al.

In addition to the work on theoretical models some groups applied numerical simulations and fitted these data to provide explicit relationships for an inverse approach [15-17]. These approaches are again restricted to equibiaxial stress states. A fully numerical inverse approach was presented by Bocciarelli and Maier [18], where it has been shown that the inverse solution is unique also for a general residual stress state when an imprint map, i.e. the topography of the indented surface under a general residual stress state, is provided as input to the objective function.

The goal of the present work is to illuminate the mechanics of indentation with a general but plain residual stress state, i.e. residual stresses normal to the surface are assumed to be zero. Of particular interest is the understanding and description of the nonlinearities, which are caused by different stress ratios. To this end, we concentrate on the change of the average pressure in contact at a given indentation depth, which avoids mixing up the effect in contact pressure and contact area. Thus, we exclude the discussion of pile-up effects. In this context it should be kept in mind that Suresh and Giannakopoulos have shown that it is possible to transform one into the other, i.e. for a given indentation depth a proportionality between indentation force and contact pressure exists.

The model validation is carried out using data from literature as well as experiments with bending bars made of an aluminium alloy Al2024 T351. Estimates for the effect will be given for a wide range of residual stresses and stress ratios. Furthermore, uncertainties can be derived for measurements with unknown mechanical properties, what is typically the case for example for the heat affected zone and melt zone of a welded joint.

2. Theoretical model

2.1 Finite element simulations

A three-dimensional finite element model was used, which has been validated regarding its accuracy and pre-stress application elsewhere [19]. The finite element model is presented in Fig. 1. Based on its symmetry, only a quarter of the specimen is modelled. All nodes on planes x=0, y=0, and z=0 are fixed normal in these respective directions to model the symmetry conditions. The finite element model contains 33.000 eight-node elements. The finer meshed cube under the indenter includes the plastic zone and is connected to the surrounding elastic foundation modelled with larger elements using the *TIE option available in ABAQUS 6.2. A rigid contact surface was used to model the spherical indenter.

For the following study of different pre-stress conditions, true stress-true strain curves from conventional tensile tests of Al2024 T351 given in [19] have been fitted using the power law hardening model in Eq. (1). Points on this stress-strain curve have been used as input for the calculations in form of a multi linear plastic strain-stress relation (see Table 1).

$$\sigma = \begin{cases} E\varepsilon\ , & \varepsilon \le \sigma_y / E \\ K\varepsilon^n\ , & \varepsilon > \sigma_y / E \end{cases}\ , \tag{1}$$

The material parameters are $E = 70$ GPa, $\nu = 0.3$, $\sigma_y = 343$ MPa, $K = 775$ MPa and $n = 0.159$.

During application of the pre-stress to the free element faces with normals in x-direction in step 1, the indenter follows the moving specimen surface through a small force in negative y-direction of 0.01 N. In step 2, the movement of the indenter is carried out displacement controlled to an indentation depth of 10% of the indenter radius, which is R=0.2 mm (see also Sec. 3.1).

Pre-stresses were applied for uniaxal and equibiaxial condition. From Fig. 2 we could qualitatively conclude that the effect on the force at a given depth in the case of a uniaxial pre-stress seems to be half of that for a biaxial pre-stress, what is in favour of the model of Lee and Kwon described in the following section. It is however not possible to generalize this statement without proof and the following sections will present a comprehensive discussion on its validity.

Table 1: Material input for finite element simulations for Al2024 T351.

True plastic strain	True stress (MPa)	True plastic strain	True stress (MPa)
0	343	0.0951	530
0.0051	370	0.135	560
0.0151	400	0.155	575
0.0251	421	0.195	595
0.0351	440	0.295	630
0.0451	460	0.495	700
0.0551	473	0.695	730
0.0651	490	0.795	750
0.0751	498	0.995	790

2.2 Deviatoric stress model

In the work of Lee, Kwon and co-workers [3,12,14], a simple model was used to derive the residual-stress-induced normal force as a product of the deviator-stress component parallel to the indentation axis

$$P = P_0 + P_{res} = P_0 - \frac{1+\kappa}{3}\sigma_1^{(res)} A_C , \qquad (2)$$

where A_C, P, P_0, P_{res} are the contact area, the indentation force with and without residual stresses and the additional force caused by the residual stress state, respectively. The residual stress state is defined by the values of the major and minor

residual stress component, $\sigma_1^{(res)}$ and $\sigma_1^{(res)} = \kappa\sigma_1^{(res)}$. Values of κ from -1 to 0 to 1 induce shear, uniaxial, and equibiaxial residual stress states, respectively.

When we introduce a pressure ratio as an effect of residual stresses, this leads to

$$\Pi_{Lee}(\sigma_1^{(res)}, \kappa) := \frac{P(\sigma_1^{(res)}, \kappa)}{P_0} = 1 - \frac{1+\kappa}{3}\frac{\sigma_1^{(res)}}{p_{m0}}, \tag{3}$$

where the assumption of Lee et al. [3] has been used that the contact hardness $p_{m0} := P_0 / A_{C0} = P / A_C$ is independent of the residual stress. Eq. (3) particularly predicts a zero effect for the "pure shear" residual stress state $\kappa = -1$, independent of the residual stress value. Note that an interesting application of the derivation of $\Pi(\sigma_1^{(res)}, \kappa)$ with respect to the residual stress

$$\Pi' := \left.\frac{d\Pi_{Lee}(\sigma_1^{(res)}, \kappa)}{d\sigma_1^{(res)}}\right|_{\sigma_1=0} = -\frac{1+\kappa}{3p_{m0}} \tag{4}$$

is the determination of the contact pressure from the measured slope Π'.

2.3 J2-flow model

With reference to the coordinate system used in the FE simulation (see Fig. 1), we can estimate the stress component in y-direction (parallel to the indentation axis) in the indented volume from the indentation force P by

$$\sigma_2 = -p_m = -\frac{P}{A} = -\frac{P_0}{A_0} \approx -\frac{P}{\pi a^2}, \tag{5}$$

where the contact radius a can be estimated from the indentation depth assuming simply a zero pile-up/sinking in from $a \approx \sqrt{2Rh - h^2}$. Supposed that the average contact pressure is invariant [6], the indentation force can directly been related to the contact area and consequently the pressure ratio and the force ratio are identical at a given indentation depth.

If we consider a representative volume element in the symmetry axis ($x=z=0$), shear stresses are zero. The remaining three principal stress components can be evaluated using the von J_2-flow criterion

$$(\sigma_1 - \sigma_2)^2 + (\sigma_2 - \sigma_3)^2 + (\sigma_3 - \sigma_1)^2 = 2\sigma_u^2, \quad (6)$$

where the flow stress σ_u can take values in the range given by the yield stress σ_y and the maximum strength of the material. To illustrate this, the trajectory of the stress tensor can be tracked during the indentation process under different equibiaxial stress states, as plotted in Fig. 3. This graph presents a cut through the flow surface by a plane defined by the normal stress axis σ_2 and the projection of the hydrostatic pressure axis on the $\sigma_1 - \sigma_3$-plane. A biaxial stress state produces a value $\sigma_b = \sqrt{2}\sigma_1$ on the x-axis of the plot, which is in our example $\sigma_{b,0} = \sqrt{2} \cdot 200\,\text{MPa}$ after application of the pre-stress.

When the contact pressure increases, σ_2 becomes increasingly negative as given in Eq. (5) and the stress tensor moves nearly radial towards the lower side of the yield surface. Once it hits the yield surface, the material starts to work harden with the increasing plastic deformation ($\sigma_u > \sigma_y$) and the stress tensor leaves the initial yield surface. With increasing indentation force the hydrostatic stress $p = (\sigma_1 + \sigma_2 + \sigma_3)/3$ takes large negative values.

Figure 3 indicates for the onset of plastic flow a linear effect caused by the equibiaxial residual stresses, as it is known from existing theoretical models, such as Lee et al. in Eq. (3). When we leave the $\sigma_1 = \sigma_3$ plane, i.e. $\kappa < 1$, the J2 flow theory however suggests a nonlinear effect as a result of the cylindrical shape of the flow rule.

In order to understand the effect of the residual stress field on the contact pressure we consider the following scenario. Similar to Fig. 3 we start to increase the force on the indenter from a stress free state (0). During loading the yield surface is hit and the material work hardens until we reach state (i) at a given indentation depth, where the diameter of the flow surface has been considerably increased from σ_y to σ_u. Now we superimpose a residual stress in form of an equibiaxial tensile stress $\sigma^{(res)}$, which brings the stress tensor outside of the yield surface. Because in plasticity theory the stress tensor is not allowed to leave the yield surface the solution enforces the superposition of a differential contact pressure $p_m^{(res)}$ to bring the stress tensor back onto the yield surface in state (ii). Note that the value of σ_u is of importance because it defines the curvature of the flow surface, which is of relevance for non-equibiaxial residual stress states. In the equibiaxial case σ_u may considerably change from tensile to compressive residual stress states due to different amounts of plastic deformation and work hardening.

The average contact pressure $p_m^{(i)}$ in the residual stress free state (i) can be taken from the experimental data, finite element simulations or an expanding cavity model as described in detail in [20,21]. Because we are considering a highly work hardened volume in the core, σ_u is the strength at a large plastic strain. Considering that the relevant subsurface volume reaches plastic strains of up to 50%, the concept of representative plastic strain [22], which is a global characteristic value, can not be applied here and we assume for simplicity of our model that $\sigma_u = K$, which is the strength at 100% strain (see Eq. (1)). We want to focus moreover on the model development, while a discussion on the error caused by uncertain estimation of σ_u will follow in Sect. 4.2.

Because of the elastoplastic compression of the subsurface volume, the stress state (i) is located on the lower side of the flow cylinder defined by the intersection of the plane $\sigma_2 = -p_m^{(i)} = -p_{m0}$ and Eq. (6) yielding

$$\sigma_2^{(i)} = -p_m^{(i)},\ \sigma_1^{(i)} = \sigma_3^{(i)} = \sigma_u - p_m^{(i)}. \tag{7}$$

In the next step we consider residual stresses in directions 1 and 3, denoted by $\sigma_1^{(res)}$ and $\sigma_3^{(res)}$ to the stress state (i) and correct the pressure level $p_m^{(ii)} = -\sigma_2^{(ii)}$ to fulfil the flow rule Eq. (5). The stress state (ii) in 1- and 3-direction is then given by

$$\sigma_1^{(ii)} = \sigma_1^{(i)} + \sigma_1^{(res)} = \sigma_u - p_m^{(i)} + \sigma_1^{(res)}, \tag{8a}$$

$$\sigma_3^{(ii)} = \sigma_3^{(i)} + \sigma_3^{(res)} = \sigma_u - p_m^{(i)} + \kappa\sigma_1^{(res)}. \tag{8b}$$

In 2-direction normal to the surface we obtain from of Eq (6) the inverse solution

$$\sigma_2^{(ii)} = \frac{1+\kappa^{(ii)}}{2}\sigma_1^{(ii)} - \left[\left(\frac{1+\kappa^{(ii)}}{2}\sigma_1^{(ii)}\right)^2 - \left((\kappa^{(ii)})^2 - \kappa^{(ii)} + 1\right)(\sigma_1^{(ii)})^2 + \sigma_u^2\right]^{1/2}, \tag{8c}$$

where $\kappa^{(ii)} = \sigma_3^{(ii)} / \sigma_1^{(ii)}$. Finally, the pressure ratio is being calculated from

$$\Pi_{J2} = \sigma_2^{(ii)} / \sigma_2^{(i)}. \tag{8d}$$

Plotting Eq. (3), the results from model (8a-8d) along with the results from our finite element simulations for Al 2024 T351 at a constant indentation depth $h/R = 0.1$, we obtain the graph presented in Fig. 5. For these calculations $p_{m0} = 1426$ MPa was calculated from Eq. (5) using the force and indentation depth obtained from the finite element simulation without residual stresses.

Both models represent linear relationships for $\kappa = 1$ but the resulting slopes are different. It should be noted, that both models are equivalent, when $\sigma_1^{(ii)} = \sigma_1^{(res)}$, $\sigma_3^{(ii)} = \kappa\sigma_1^{(res)}$, $\kappa^{(ii)} = \kappa = 1$, i.e. the stress state is evaluated at the initial state (o) and the loading trajectory (o)-(i) is ignored. Then we would obtain the solutions

$\Pi_{Lee} = 1-(2\sigma_1)/(3p_{m0})$ and $\Pi_{J2} = 1-\sigma_1 / p_{m0}$, which both can be found in [13] and [6], respectively. While Lee and Kwon suspected the reason for this difference in an improper definition of the differential contact stress in [6], our model motivated by plasticity theory is in favour to the work of Suresh and Giannakopoulos.

The remaining nonlinearity in the finite element results for the equibiaxial case are supposed to reflect the different amounts of work hardening reached for different residual stresses. A residual stress of -200 MPa, 0 MPa and 200 MPa produces an equivalent plastic strain of 43%, 30% and 21% in the subsurface volume examined in Fig. 3, respectively. Consequently, the strengths $\sigma_u^{(i)}$ and $\sigma_u^{(ii)}$ indicated in Fig. 4 represent Mises cylinders of different diameter dependent on the current amount of work hardening.

For values of $\kappa < 1$, Eq. (8) fits the finite element results much better than the linear model given in Eq. (3) and correctly accounts for the nonlinear effects in the pressure ratio. In particular it predicts the unsymmetric effect for the uniaxial case, which has been observed experimentally by Tsui et al. [1] and furthermore predicts a non-zero effect for the pure shear case $\kappa = -1$ that has not been reported elsewhere so far.

3. Experimental validation

3.1 Experimental details

Indentation experiments have been performed using a testing machine ZHU0.2/Z2.5, which is equipped with the hardness measuring head and a certified Rockwell indenter with a tip radius of $R = 0.2$ mm (Zwick Roell AG, Ulm, Germany). The built-in load cell measures applied forces between 2 N and 200 N with the force resolution of 0.01 N and displacement resolution of 0.02 µm.

The tests have been performed on a rolled high strength aluminium alloy 2024 T351 frequently used in airplanes. The specimens are prepared by cutting a large plate in the mid-plane of the plate thickness direction in order to eliminate the property gradient which might exist along the plate thickness direction. The thickness of the specimen is around 10 mm with surface dimension being large enough so that boundary effects can be neglected. The specimen were mechanically polished with sequential abrasive paper from 80 grades down to 2400 grade followed by diamond polishing with abrasive grit sizes of 3 µm and finalized with polishing using SiO_2 solution of 0.05 µm.

To simulate a residual stress inside the test specimens, the specimens were loaded with a well defined external force. Two rectangular beam-specimens were fixed to a steel block. At the free end of the beams a force, which is measured via a load-cell, can be subjected to the beams via a screw in order to produce a bending moment. The resulting uniaxial pre-stress was always kept below the elastic limit of the material to avoid plastic deformation by means of controlling the application force into the beams. The stress calculation was done by employing the free-body diagram and considers the beam clamped at one end (cantilever beam) and subjected to a force *P* at the free end. A schematic drawing of this specimen assembly is given in Figure 6.

3.2 Results

The measured force-depth curves were fitted with a power-law function to allow a simple interpolation of force values to the same indentation depth. All fit parameters and the resulting pressure ratio at a given indentation depth of 20 µm are listed in Table 2 along with the applied pre-stresses.

In Fig. 7 the experimental data points are given in form of the average value of Π and the standard deviation for three selected indentation depths $h/R \in \{0.005, 0.025, 0.1\}$. The observed variation concerning the effect of indentation depth are small and below the model uncertainties so that our model Eq. (8) as well as the finite element results very well agree with the experimental measurements.

Table 2. Force-depth curves for uniaxially pre-stressed ($\kappa = 0$) Al2024 T351 alloy.

σ_1(MPa)	$P(h)$ (N)	$P(h = 0.1R)$ (N)	$\Pi_{J2}(h = 0.1R)$
-140	$4352 \cdot h^{1.230}$	35.40	1.028
-130	$4293 \cdot h^{1.225}$	35.61	1.034
-125	$4266 \cdot h^{1.219}$	36.22	1.052
-120	$4541 \cdot h^{1.239}$	35.66	1.036
-100	$4711 \cdot h^{1.246}$	35.99	1.045
-90	$4159 \cdot h^{1.216}$	35.73	1.038
-80	$4214 \cdot h^{1.223}$	35.23	1.023
0	$4119 \cdot h^{1.223}$	34.43	1
80	$4175 \cdot h^{1.235}$	33.30	0.967
90	$3967 \cdot h^{1.226}$	32.77	0.952
100	$3960 \cdot h^{1.224}$	32.97	0.958
120	$3693 \cdot h^{1.209}$	32.61	0.947
125	$3870 \cdot h^{1.218}$	32.99	0.958
130	$3537 \cdot h^{1.206}$	31.60	0.918
140	$3972 \cdot h^{1.233}$	31.93	0.927

4. Discussion of prediction and identification capabilities

4.1 Prediction of residual stress effect and errors

Combining Eqs. (5-8), a predictive model for the effect of a general residual stress state on the indentation force results, where $P^{(res)}/P^{(0)} = \Pi_{J2}(p_m, \sigma_u, \sigma_1^{(res)}, \kappa)$. The quality of this simple model in predicting the effect on the indentation force for the complete loading curve is demonstrated exemplarily in Fig. 8. A noticeable

deviation is visible only for the case of equibiaxial compression at large indentation depths. This deviation has been discussed in the context of Fig. 5 and is supposed to be caused by work hardening of the material.

For practical applications, it is useful to estimate the error in hardness measurements induced by residual stress states, such as for the evaluation of hardness profiles along welds, as it has for example been done in [23] for friction stir welds. Since both, hardness and strength of the material influence the effect due to residual stresses, the error

$$err(p_{m0}/\sigma_u, \sigma_1^{(res)}/\sigma_u, \kappa) = \Pi_{J2} - 1 \qquad (9)$$

is material dependent and can perhaps be neglected for a certain material while it may be significant for others.

For our example material Al2024 T351, the calculated value of $p_{m0}/\sigma_u = 1.8$ at an indentation depth of $h/R = 0.1$ is identical for the experimental value, finite element result, as well as the expanding cavity model [21]:

$$p_m/\sigma_u = (2/3)[(1-1/n) + (1/n + 3/4)(Ea/4R\sigma_y)^n](\sigma_y/\sigma_u)\,. \qquad (10)$$

The error calculated from (9) can then be reduced to $err(\sigma_1^{(res)}/\sigma_u, \kappa) = \Pi_{J2} - 1$ when we discuss the error sensitivity for a given material, such as Al2024-T351. The results plotted in Fig. 9 represent an error map when we determine the hardness for an unknown residual stress state including in particular the ratio of the residual stress components, κ. While for thin films κ is typically 1 it can significantly vary in welds from negative to positive values. For instance, values of ($\sigma_1^{(res)} = 75$ MPa , $\kappa = -1$) and ($\sigma_1^{(res)} = 150$ MPa , $\kappa = 0.2$) have been measured by neutron diffraction in the regions of run-in and run-out of a laser beam weld, respectively [24]. In friction stir welds, values of $\kappa = -1$ at a stress $\sigma_1^{(res)} = 60$ MPa have for example been observed in the thermally affected zone [25].

It should be noted that these residual stresses have been measured by neutron diffraction inside the volume of welded components. By cutting a cross-section, residual stresses will be partially released so that the following discussion should be understood being conservative. A more precise investigation of the residual stress state in the indented cross-section of a friction stir weld will therefore be subject of a subsequent paper. Using the available values mentioned above, the expected error in the measured hardness can be taken from Figure 9, assuming the strength of the base material $\sigma_u = K = 775$ MPa.

In both types of welding, the material undergoes however a significant softening through precipitation growth and dissolution in and near the welding zone, which moves both points further away from $\sigma_1^{(res)} / \sigma_u = 0$ and therefore to larger error values and might partially compensate the overestimation by taking volume residual stresses. Figure 9 can in this way also be used to assess the uncertainty in the materials strength σ_u as a result of an under- or overmatch on the measured hardness. It can be seen that there exist large areas, where a significant change of σ_u has an effect below 5%. Also the the assumption $\sigma_u = K$, which has been introduced in our model, increases the ratio $\sigma_1^{(res)} / \sigma_u$ by 10 to 20%, causing only a significant underestimation of the residual stress effect in the lower left corner of the error map as it is evident from Fig. 9.

4.2 Identification of mechanical strength

That the strength σ_u sufficiently represents the mechanical properties of a material in order to predict the effect of a residual stress state on the contact pressure, which is one of the most important results of the previous discussion. This allows on one hand to estimate the uncertainty in hardness measurements for a

material, which has been modified e.g. through a welding process. On the other hand, one can use hardness tests to find the value of σ_u. For many materials it is not possible to measure this value from simple tensile experiments because necking and fracture typically occur in an earlier state, i.e. $\sigma_{UTS}(=R_m) < \sigma_u$.

In contrast to the model of Suresh and Giannacopoulos, which requires explicit data on the true contact area, our model is capable of fitting the hardness data provided by Tusi et al. [1] by a simple adjustment of the value σ_u in Eq. (8). The objective function, based on a reference average pressure $p_m(\sigma^{(res)}=0)=1.3$ GPa, is plotted in Fig. 10. Note that the reference average pressure has been obtained by averaging the hardness data in a stress range between -50 MPa and 50 MPa. The result of the fit yields a maximum (true) strength of $\sigma_u = 710$ MPa. Plotting Eq. (8) for the identified value of σ_u along with the data published by Tsui et al. in Fig. 11 shows the good agreement of our model with these data once more validating that the observed nonlinearity in the measured hardness is attributed to the shape of the flow rule.

5. Conclusions

The effect of residual stresses in hardness measurements is an important problem which has been discussed extensively over the last decade. Beside some empirical and numerical approaches three major models have been developed so far, where two of them are restricted to equibiaxial residual stress states while one of them accounts for a general residual stress state but is not able to describe the well-known nonlinearity. The derived models are often used for inverse approaches in order to determine the residual stress from hardness measurements.

The simple theoretical model, which has been proposed in this paper, analyzes the von Mises yield surface at the stress states, which are produced in a volume underneath the indenter without and with residual stresses. The resulting relationship covers arbitrary stress ratios and predicts the known nonlinearity for the uniaxial stress state and also the so far unknown non-zero effect for the pure shear stress state.

The finite element data suggest that the nonlinearity in the equibiaxial case, which has also been found by Tsui et al. is caused from the hardening behaviour of the material while for other stress states the dominant source for nonlinearities is the shape of the von Mises flow surface in the principle stress space. Because the size of the flow surface is described by the strength at the current state of plastic deformation, the maximum strength reached at the considered indentation depth is another required parameter. Errors caused by difficulties in estimating this value can be estimated from the model.

For future practical applications, error maps can be provided which easily allow estimating the error in the measured indentation force for unknown residual stress states or unknown maximum strength. The latter is in particular important, when the material has undergone a significant modification, for example through welding processes. Beyond the uncertainties of the experimental technique, the most important uncertainty is the residual stress ratio κ when compressive residual stresses are present. An inverse approach towards the determination of the residual stress at an uncertain stress ratio will therefore be limited to tensile residual stresses.

References

[1] Tsui TY, Oliver WC, Pharr GM. J. Mat. Res. 1996;11:752.

[2] Bolahskov A, Oliver WC, Pharr GM. J. Mat. Res. 1996;11:760.

[3] Lee Y-H, Kwon D. Scripta Mat. 2003;49:459.

[4] Zhao M, Chen Xi, Yan J, Karlsson AM. Acta Mat. 2006;54:2823.

[5] Xu Z-H, Li X. Acta Mat. 2005;53:1913.

[6] Suresh S, Giannakopoulos AE. Acta Mat. 1998;46:5755.

[7] Carlsson S, Larsson P-L. Acta Mat. 2001;49:2179.

[8] Swadener JG, Taljat B, Pharr G-M. J. Mat. Res. 2001;16:2091.

[9] Carlsson S, Larsson P-L, Acta Mat. 2001;49:2193.

[10] Larsson P-L. Phil. Mag. 2006;86:5155.

[11] Larsson P-L. J. Mater. Proc. Techn. 2007;184:372.

[12] Lee Y-H, Kwon D. Mat. Sci. Forum 2004;449-452:93.

[13] Lee Y-H, Kwon D. Acta. Mat. 2004 ;52 :1555.

[14] Lee Y, Kim J-Y, Lee J-S, Kim K-H, Koo JY, Kwon D. Phil. Mag. 2006 ;21: 5497.

[15] Chen X, Yan J, Karlsson AM. Mat. Scie. Eng. A 2006;416:139.

[16] Chen K-S, Chen T-C, Ou K-S. Thin Solid Films 2008;516:1931.

[17] Yan J, Chen X, Karlsson AM. J. Eng. Mat. Techn 2007;129:200.

[18] Bocciarelli M, Maier G. Comput. Mat. Science 2007;39:381.

[19] Heerens J, Mubarok F, Huber N. submitted for publication, 2008.

[20] Johnson KL. J. Mech. Phys. Solids 1970;18:115.

[21] Ai K, Dai LH. Scripta Mat. 2007;56:761.

[22] Tabor D. The Hardness of Metals, Oxford University press, 2000.

[23] Amancio S, Sheikhi S, dos Santos J, Bolfarini C. J. Mater. Processing Techn. 2008;doi:10.1016/j.jmatprotec.2007.12.008.

[24] Bayraktar FS, Staron P, Kocak M, Schreyer A. Mat. Science Forum 2008; 571-572:355.

[25] Staron P, Kocak M, Williams S. Appl. Phys. A 2002;74:1161.

List of figure captions

Figure 1. Three dimensional finite element model for indentation simulations with applied uniaxial or equibiaxial pre-stress $\sigma^{(res)}$.

Figure 2. Force-depth curves for different pre-stress conditions of $\sigma^{(res)} = 200$ MPa magnitude.

Figure 3. Effect of an equibiaxial pre-stress on the stress trajectory in a subsurface volume.

Figure 4. Illustration of the effect of an equibiaxial residual stress state on the indentation contact pressure.

Figure 5. Comparison of finite element results (markers) with Eq. (3) and Eq. (8).

Figure 6. Sketch of specimen installation for measuring the effect of uniaxial pre-stress using indentation testing.

Figure 7. Experimental validation of model Eq. (8) for the uniaxial case ($\kappa = 0$).

Figure 8. Prediction of the residual stress effect over the whole loading curve for Al2024-T351.

Figure 9. Predicted error in % for hardness measurements of Al2024 T351 alloy ($p_{m0} / \sigma_u = 1.8$).

Figure 10. Objective function for fit of model Eq. (8), denoted by p_m to the data of Tsui et al., denoted by H in the objective function Err.

Figure 11. Hardness data of Tsui et al. ($\kappa = 0$) and fit of model Eq. (8) for $\sigma_u = 710$ MPa.

Figures

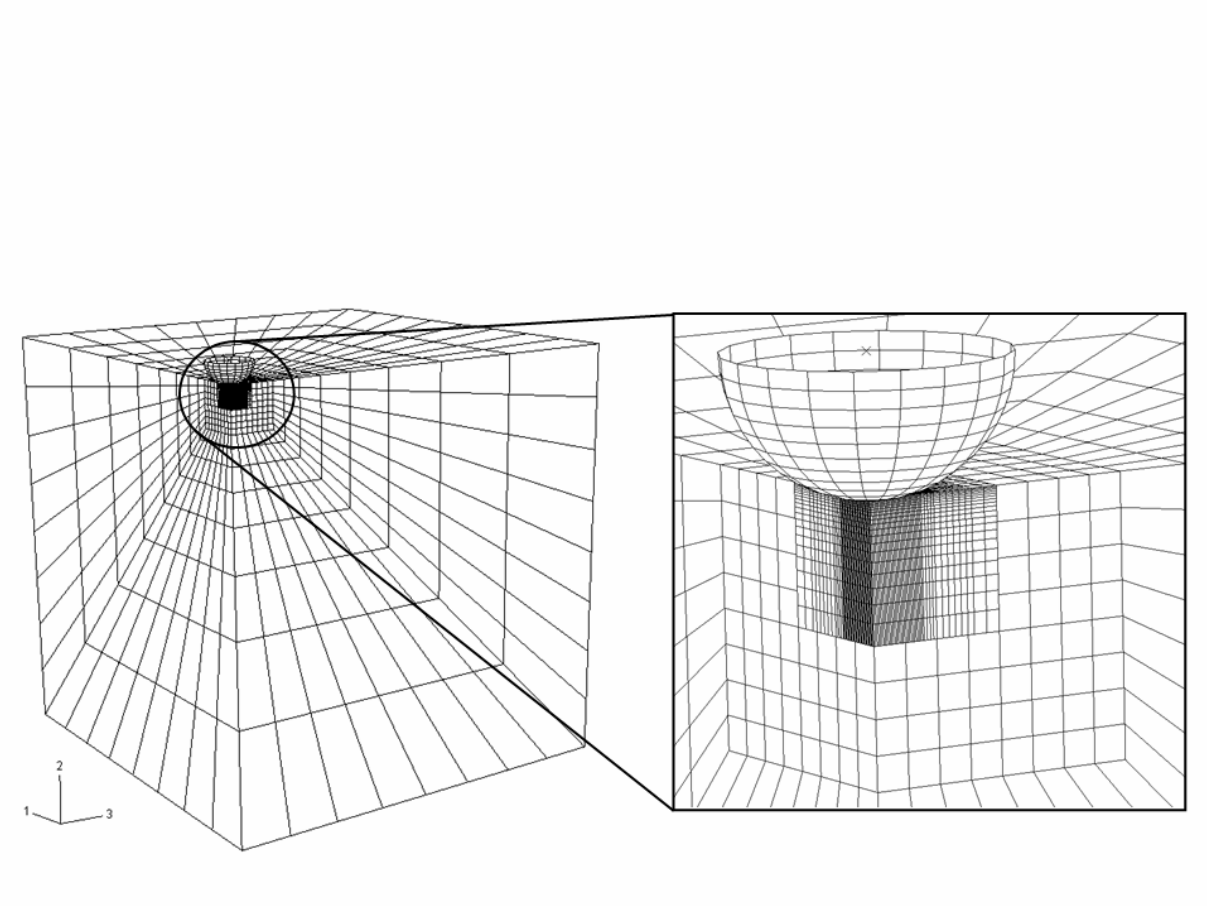

Figure 1. Three dimensional finite element model for indentation simulations with applied uniaxial or equibiaxial pre-stress $\sigma^{(res)}$.

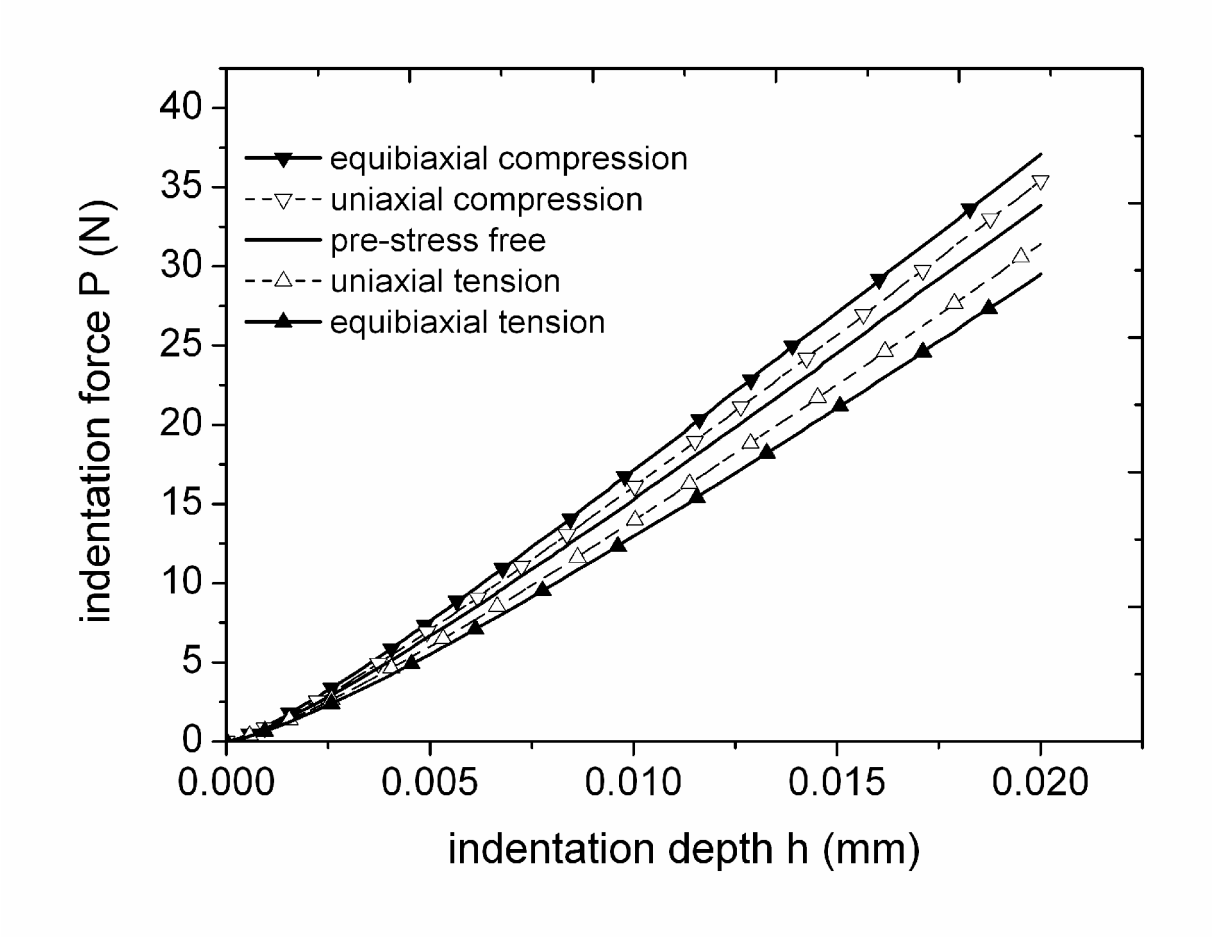

Figure 2. Force-depth curves for different pre-stress conditions of $\sigma^{(res)} = 200$ MPa magnitude.

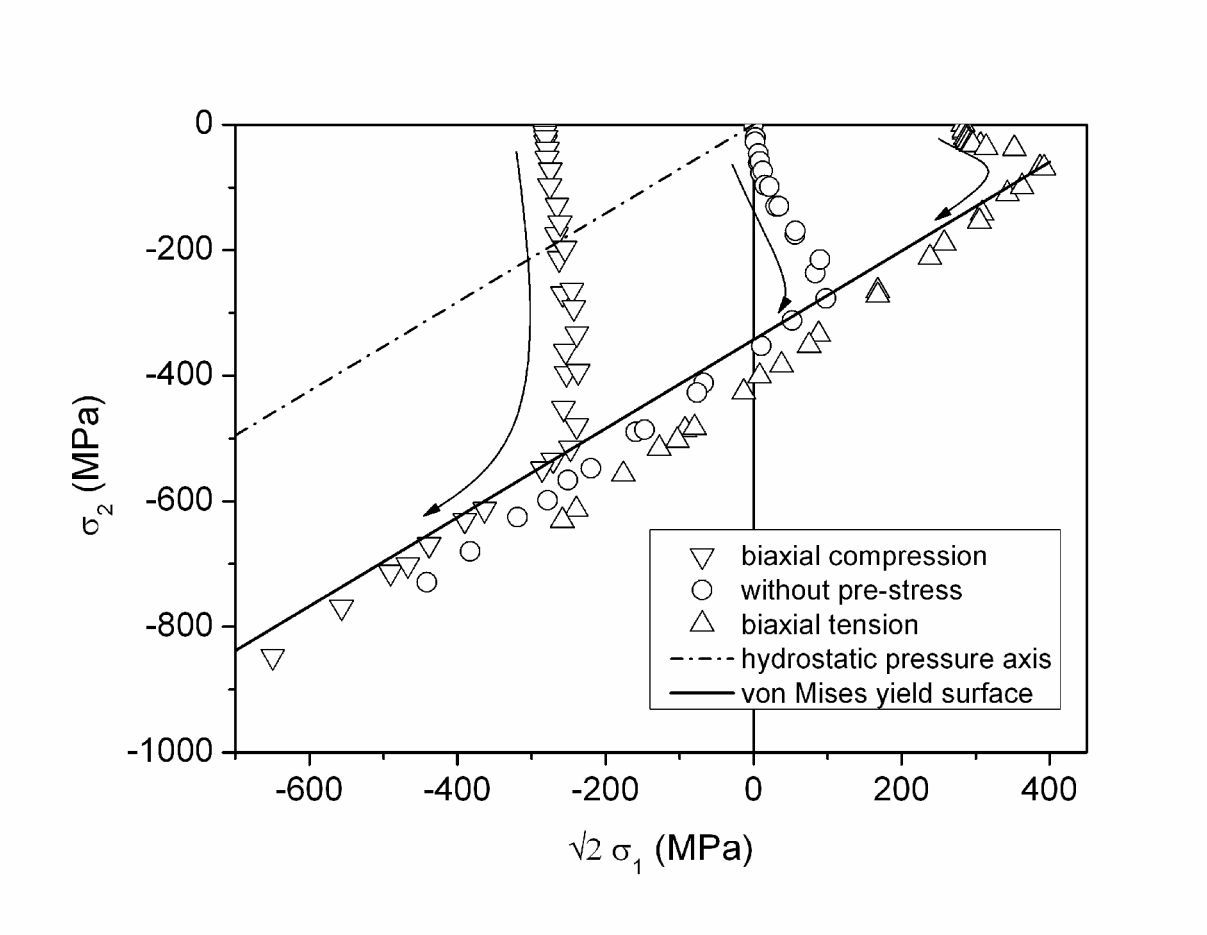

Figure 3. Effect of an equibiaxial pre-stress on the stress trajectory in a subsurface volume.

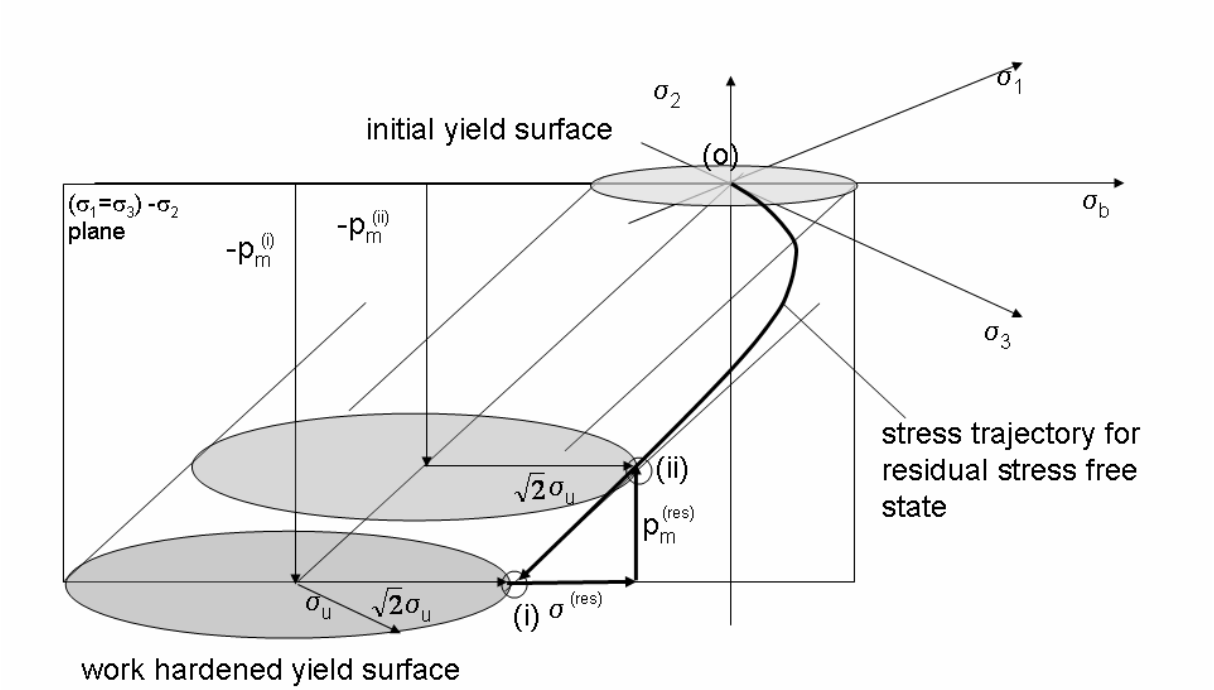

Figure 4. Illustration of the effect of an equibiaxial residual stress state on the indentation contact pressure.

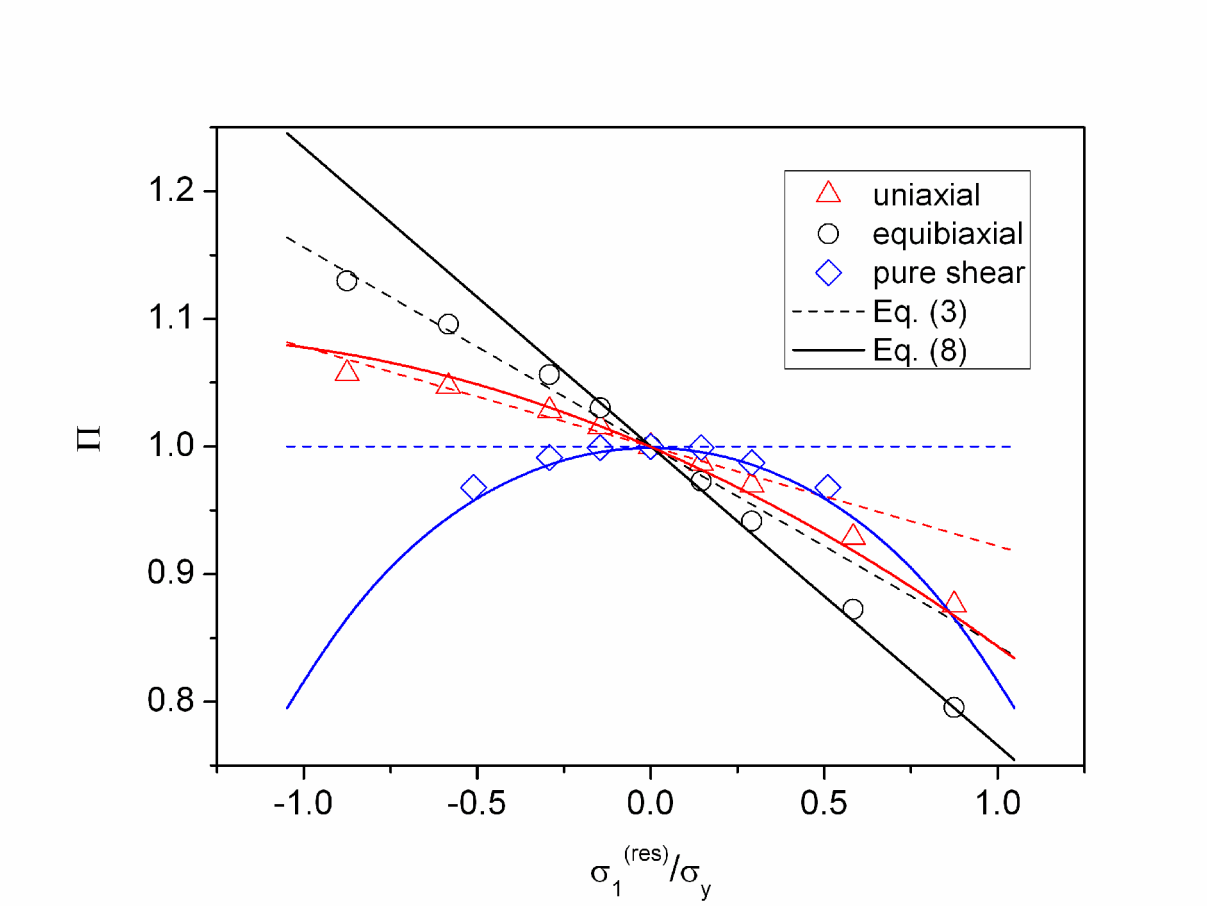

Figure 5. Comparison of finite element results (markers) with Eq. (3) and Eq. (8).

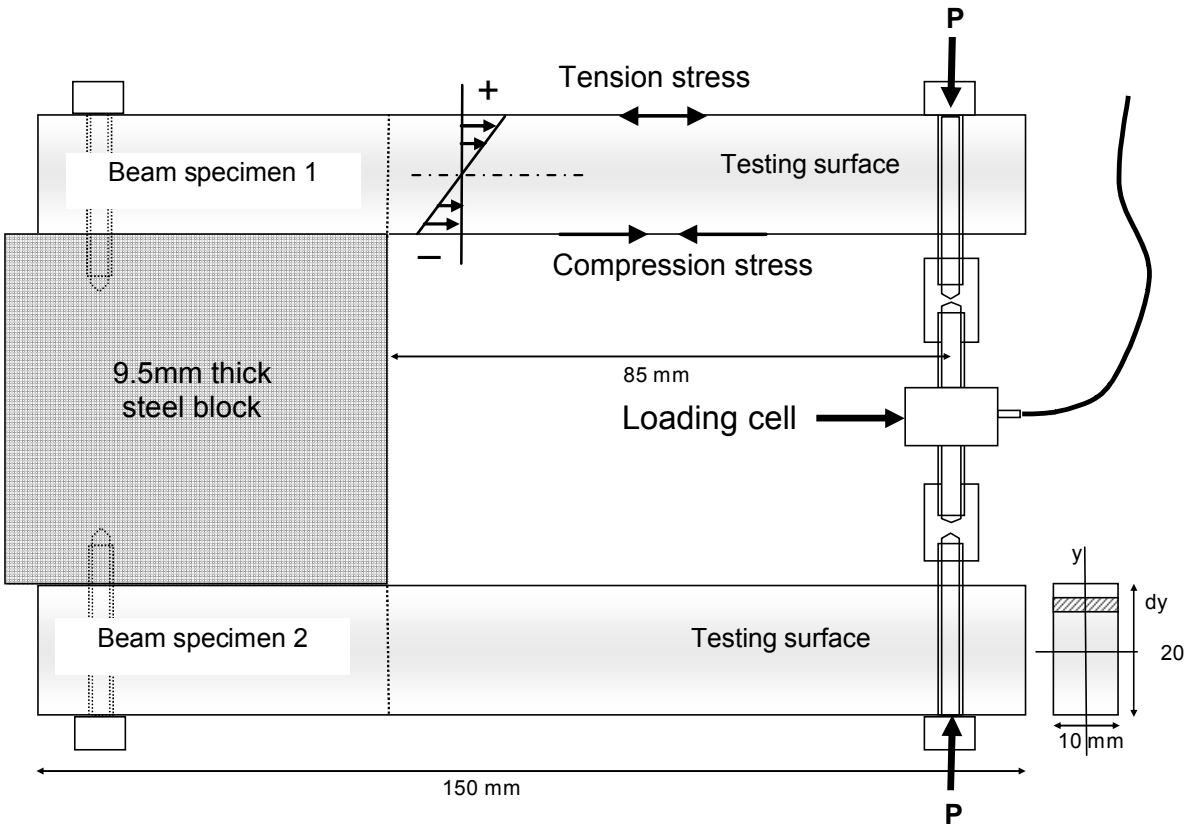

Figure 6. Sketch of specimen installation for measuring the effect of uniaxial pre-stress using indentation testing.

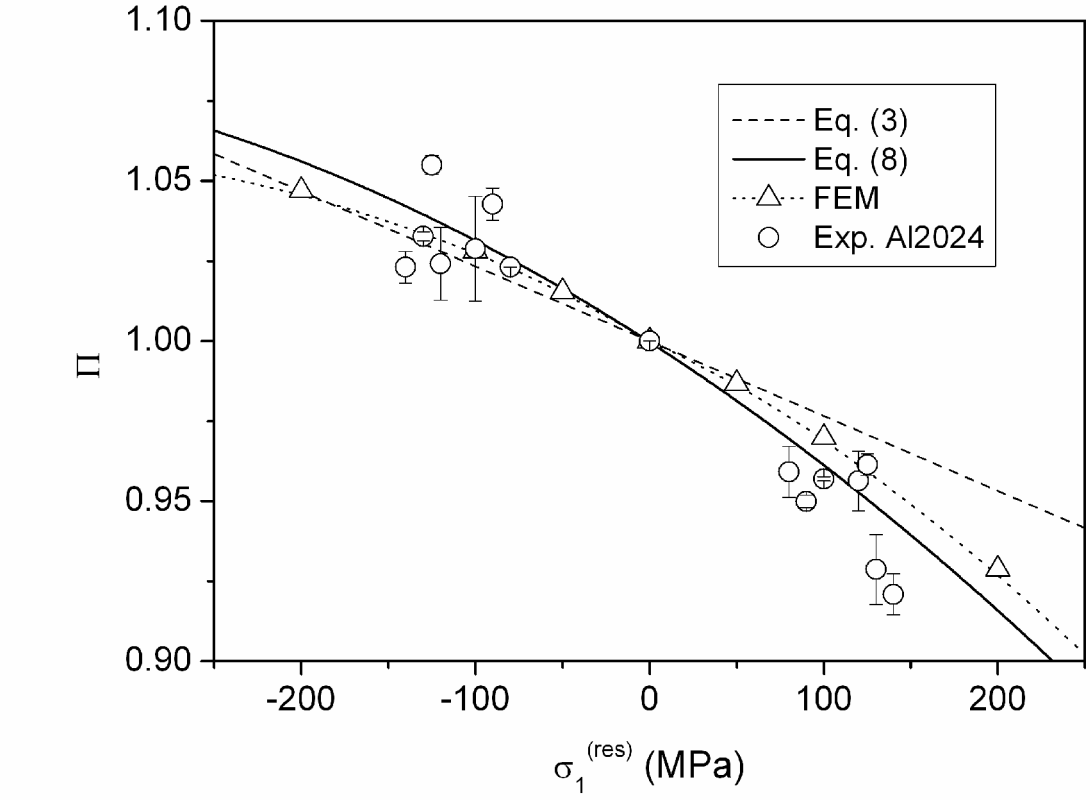

Figure 7. Experimental validation of model Eq. (8) for the uniaxial case ($\kappa = 0$).

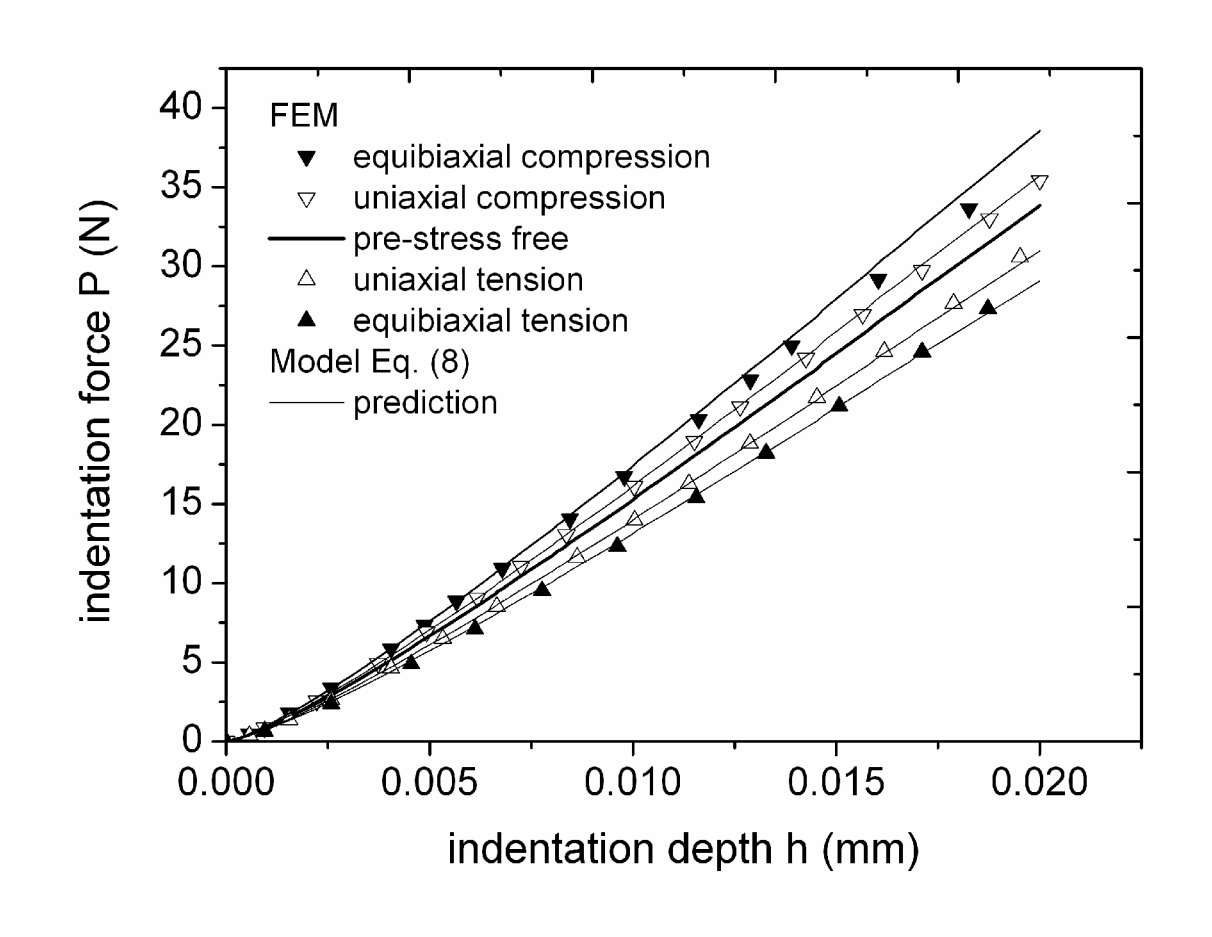

Figure 8. Prediction of the residual stress effect over the whole loading curve for Al2024-T351.

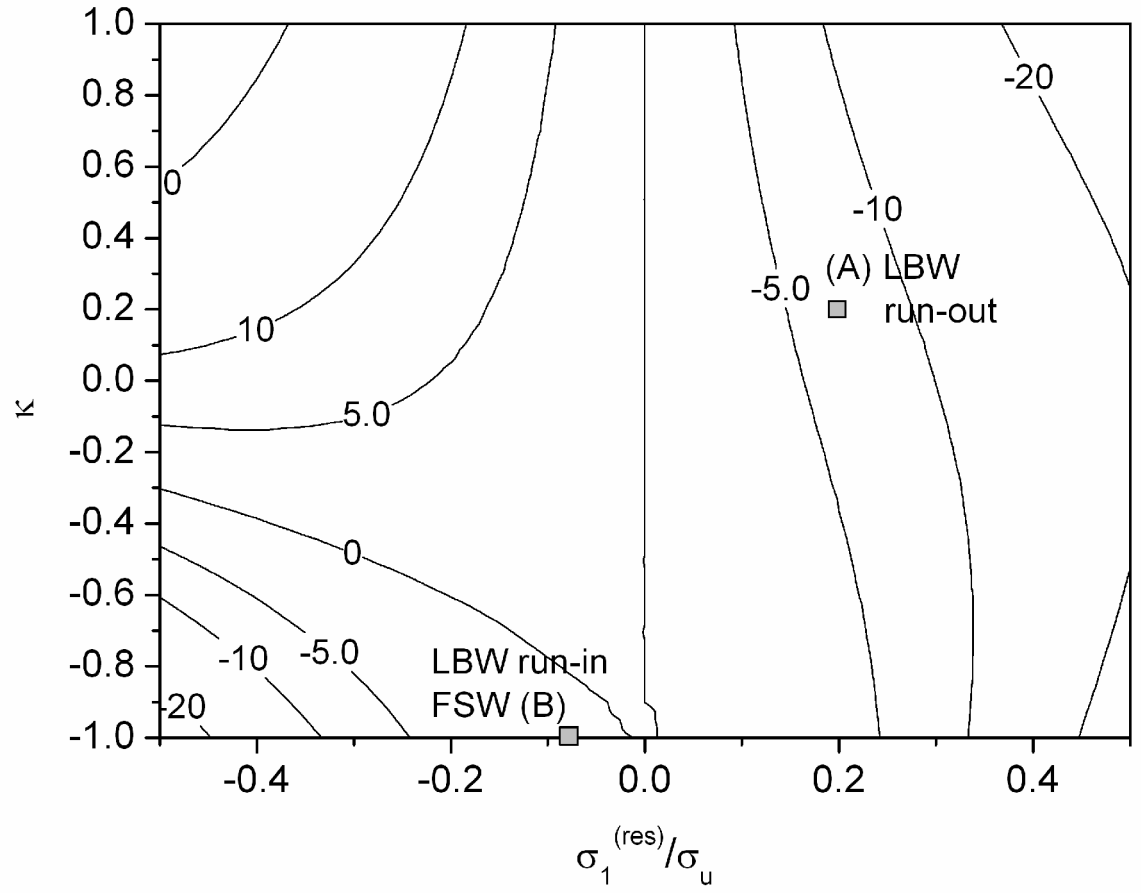

Figure 9. Predicted error in % for hardness measurements of Al2024 T351 alloy ($p_{m0}/\sigma_u = 1.8$).

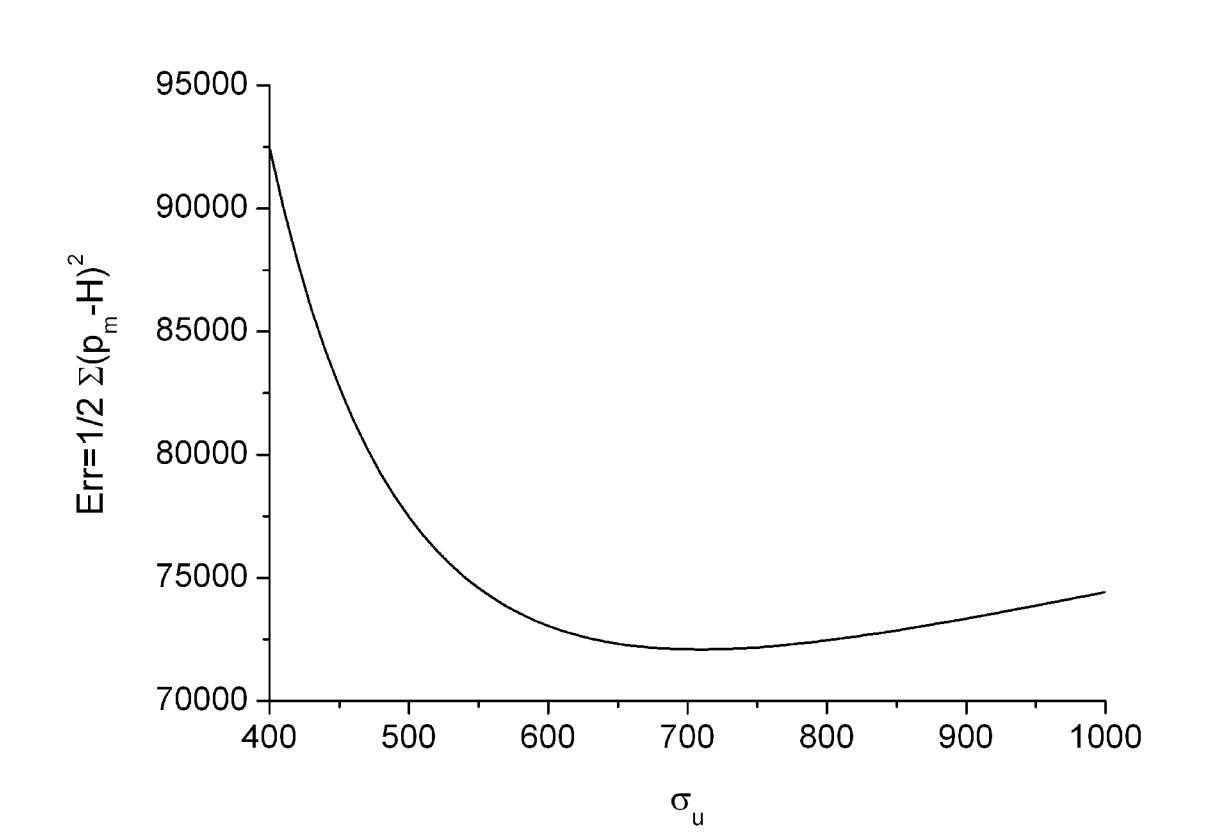

Figure 10. Objective function for fit of model Eq. (8), denoted by p_m to the data of Tsui et al., denoted by H in the objective function Err .

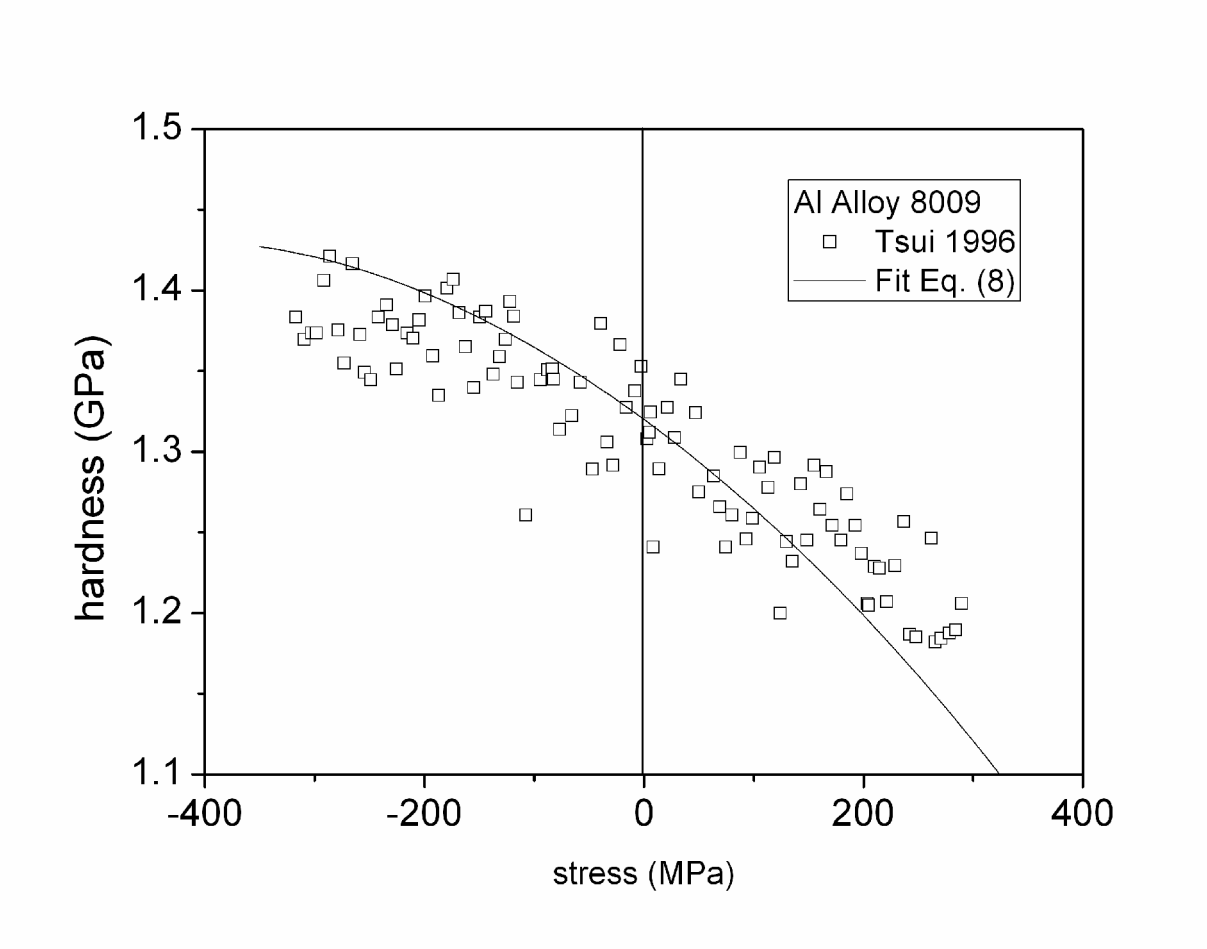

Figure 11. Hardness data of Tsui et al. ($\kappa = 0$) and fit of model Eq. (8) for $\sigma_u = 710$ MPa.